PAPER

Accuracy Improvement in DOA Estimation with Deep Learning*

Yuya KASE[†a)], *Student Member*, Toshihiko NISHIMURA[†], *Senior Member*, Takeo OHGANE[†b)],
Yasutaka OGAWA[†], *Fellows*, Takanori SATO[†], *Member, and* Yoshihisa KISHIYAMA[††], *Senior Member*

SUMMARY   Direction of arrival (DOA) estimation of wireless signals is demanded in many applications. In addition to classical methods such as MUSIC and ESPRIT, non-linear algorithms such as compressed sensing have become common subjects of study recently. Deep learning or machine learning is also known as a non-linear algorithm and has been applied in various fields. Generally, DOA estimation using deep learning is classified as on-grid estimation. A major problem of on-grid estimation is that the accuracy may be degraded when the DOA is near the boundary. To reduce such estimation errors, we propose a method of combining two DNNs whose grids are offset by one half of the grid size. Simulation results show that our proposal outperforms MUSIC which is a typical off-grid estimation method. Furthermore, it is shown that the DNN specially trained for a close DOA case achieves very high accuracy for that case compared with MUSIC.

key words: *DOA estimation, deep learning, machine learning*

1. Introduction

Direction of arrival (DOA) estimation of radio signals is a technique required for user localization in various target tracking applications and becomes important in recent mobile communication systems. For these several decades, it has been common to use an antenna array for DOA estimation instead of narrow beam antennas. Thus, many signal processing techniques, e.g., beamforming, Capon, multiple signal classification (MUSIC), estimation of signal parameters via rotational invariance techniques (ESPRIT), have been investigated [3].

In recent years, compressed sensing has been applied to the DOA estimation field [4]. Compressed sensing is a technique exploiting sparseness of the solution in the target vector space [5]. In DOA estimation, the number of arrivals is much fewer than the number of angle domain grids in general if we divide the angle space into small angle bins. Thus, the compressed sensing technique is applicable to DOA esti-

mation, and it has been reported that DOA estimation using a compressed sensing solver called half-quadratic regularization (HQR) shows higher accuracy compared with MUSIC in the case of multi-band signals [6].

The compressed sensing technique is classified as on-grid (discrete) estimation. This means that the estimated DOA angles are quantized on a pre-determined grid in the angle domain. Thus, quantized distortion is inevitable unlike the general DOA estimation methods classified as off-grid (continuous) estimation such as MUSIC. However, if such quantized distortion is acceptable, the on-grid estimation is attractive because other recent discrete estimation algorithms can be applied.

Deep learning or machine learning is a typical application suitable for on-grid estimation problems. The deep neural network (DNN) proposed by Hinton et al. [7], [8] has been extensively studied in the fields of images, sounds, languages, and so on. Although DNN requires a large amount of calculations during the training phase, estimation using the trained DNN is performed with mainly matrix-vector multiplications, and thus the computational complexity in estimation phase is lower than the ones of MUSIC (requiring eigenvalue decomposition) and HQR (requiring a number of inverse matrix calculations) when the vector size is large. In addition, the advantage that we can design the DNN for specific scenarios such as rare but severe cases is unique to machine-learning-based estimation. Thus, in this paper, we focus on DOA estimation using deep learning.

DOA estimation using deep learning was first applied in the speech source localization field [9]. [10] uses a convolutional neural network (CNN) to estimate near-field sources with spherical wavefront model. In the radio resource localization field, several papers can be seen recently [11]–[15]. In [11], the DOA estimation results are used for massive multiple-input multiple-output (MIMO) channel estimation, and estimation performance related to the number of hidden layers was precisely demonstrated. The DNN proposed in [12] consists of two parts, a spatial filtering part for subregion decomposition and a spatial spectrum estimation part, and succeeds in obtaining accurate spectra. In [13], their DNN estimates DOAs under a massive MIMO system with a uniform circular array and achieves lower computational complexity while offering similar or even better performance compared with the conventional maximum likelihood method. By converting DOA estimation problem into a regression task, [14] proposes a DOA estimation framework in

the near-field MIMO system based on complex-valued residual network (ResNet). These papers discuss application-oriented performance, and the DNN configurations are not general in terms of the array size [11], [13], [14], the array geometry [13], the use of subregion decomposition [12], or the use of complex-valued network [14]. Our previous study verified the estimation capabilities of DNNs under a simple estimation situation and discussed the parallel use of a general-purpose DNN and the DNN designed for a specific scenario where two close DOA signals were incident [15]. However, [15] treats an integer DOA estimation problem. Issues of on-grid problems in the DNN have not been discussed yet in comparison to other off-grid estimation techniques.

In this paper, we analyze DOA estimation capabilities of DNNs with different numbers of layers/units using batch learning and some optimizing techniques. A comparison of DOA estimation accuracies between a deep learning based technique (on-grid estimation) and MUSIC (off-grid estimation) shows that the DNN frequently fails to estimate the correct bin when a signal arrives at angles near the grid border. As a solution for this problem, we propose a method of combining two DNNs whose grids are staggered. Furthermore, we train the DNN suitable to the close DOA case, evaluate the estimation accuracy, and propose a parallel use of multiple DNNs designed for different scenarios as in [15]. In the rest of paper, the configuration and training process of DNN are shown after formulation of the array structure and signal arrival model. Finally, performance evaluation by computer simulations is described.

2. Correlation Matrix of Array Antenna

2.1 Formulation of Received Signal

Figure 1 shows that K plane waves with a wavelength λ and complex amplitudes $s_k(t)$, $k = 1, \ldots, K$ are incident at angles θ_k, $k = 1, \ldots, K$ on an L-element uniform linear array with an element spacing of d. The received signal at the lth antenna is expressed as

$$x_l(t) = \sum_{k=1}^{K} s_k(t) e^{-j\frac{2\pi}{\lambda}(l-1)d\sin\theta_k} + n_l(t), \qquad (1)$$

where $n_l(t)$ is an additive white Gaussian noise at the lth
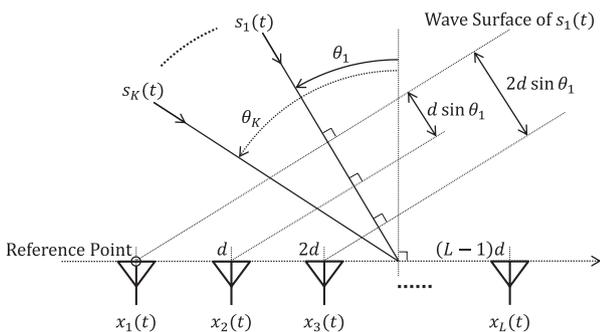
Fig. 1 An L-element uniform linear array and incident waves.

antenna.

The received signals at all the antennas can be expressed in a vector-matrix form as

$$\begin{aligned} \boldsymbol{x}(t) &= [x_1(t), x_2(t), \ldots, x_L(t)]^T \\ &= [\boldsymbol{a}(\theta_1), \boldsymbol{a}(\theta_2), \ldots, \boldsymbol{a}(\theta_K)]\, \boldsymbol{s}(t) + \boldsymbol{n}(t) \\ &= \boldsymbol{A}\boldsymbol{s}(t) + \boldsymbol{n}(t), \end{aligned} \qquad (2)$$

where $[\cdot]^T$ denotes the transpose. $\boldsymbol{x}(t)$, $\boldsymbol{s}(t)$, and $\boldsymbol{n}(t)$ are the received signal vector, transmit signal vector, and noise vector, respectively. $\boldsymbol{a}(\theta)$ is a mode vector of which lth entry is $\exp(-j\frac{2\pi}{\lambda}(l-1)d\sin\theta)$, and $\boldsymbol{A}$ denotes a mode matrix with K mode vectors as columns.

The $L \times L$ correlation matrix of $\boldsymbol{x}(t)$ is expressed as

$$\boldsymbol{R}_{xx} = E\left[\boldsymbol{x}(t)\,\boldsymbol{x}^H(t)\right] = \boldsymbol{A}\boldsymbol{S}\boldsymbol{A}^H + \sigma^2\boldsymbol{I}, \qquad (3)$$

where $E[\cdot]$, $[\cdot]^H$, and $\boldsymbol{I}$ denote the ensemble average, the conjugate transpose, and the identity matrix, respectively. $\boldsymbol{S} = E\left[\boldsymbol{s}(t)\,\boldsymbol{s}^H(t)\right]$ is the $K \times K$ signal correlation matrix, and σ^2 is the noise power. Note that this $\boldsymbol{R}_{xx}$ is a Hermitian matrix.

2.2 DOA Estimation Based on MUSIC

The rank of $\boldsymbol{A}\boldsymbol{S}\boldsymbol{A}^H$ is K at most. Then, the eigenvectors corresponding to the $(L - K)$ smallest eigenvalues of $\boldsymbol{R}_{xx}$ span the noise subspace which is orthogonal to the signal subspace. MUSIC is a typical technique based on subspace projection. It is written as a problem of finding θ which satisfies

$$\sum_{\nu=K+1}^{L} \left|\boldsymbol{a}^H(\theta)\,\boldsymbol{e}_\nu\right|^2 = 0, \qquad (4)$$

where $\boldsymbol{e}_\nu$ is the noise eigenvector.

Defining $\zeta = \exp(-j\frac{2\pi}{\lambda}d\sin\theta)$, we can rewrite Eq. (4) as

$$Q(\zeta) = \boldsymbol{p}^H(\zeta)\boldsymbol{E}_N\boldsymbol{E}_N^H\boldsymbol{p}(\zeta) = 0, \qquad (5)$$

where $\boldsymbol{p}(\zeta) = \left[1, \zeta, \zeta^2, \ldots, \zeta^{L-1}\right]^T$ is a rewrite of $\boldsymbol{a}(\theta)$ using ζ, and $\boldsymbol{E}_N$ is an $L \times (L-K)$ matrix with noise eigenvectors as columns. The method of estimating DOAs by finding the roots of Eq. (5) is particularly called Root MUSIC [16]. In this paper, Root MUSIC is used as a baseline because MUSIC is applicable to any array structures and Root MUSIC requires no peak searching. Cramér-Rao bound (CRB) [17], is also a very common baseline. However, the on-grid estimation is always distorted by quantization. Thus, the MSE comparison to the CRB is not enough to discuss the performance. This is another motivation to use Root MUSIC as a baseline. In the later part of this paper, we use the estimation success rate as an evaluation measure.

3. Application of Deep Learning

3.1 Formulation of DNN

Figure 2 shows a general single-layer dense neural network

Fig. 2 A single-layer dense neural network.

Fig. 3 A deep neural network (DNN).
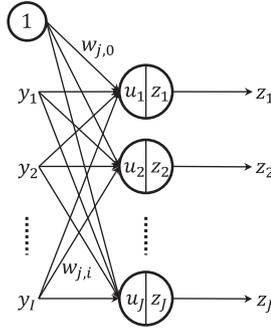
of J units with I inputs and J outputs. The J outputs z_j, $j = 1, \ldots, J$ can be expressed as

$$[z_1, z_2, \ldots, z_J]^T = [f(u_1), f(u_2), \ldots, f(u_J)]^T \quad (6)$$

$$
\begin{bmatrix} u_1 \\ u_2 \\ \vdots \\ u_J \end{bmatrix} = \begin{bmatrix} w_{1,0} & w_{1,1} & \cdots & w_{1,I} \\ w_{2,0} & w_{2,1} & \cdots & w_{j,I} \\ \vdots & \vdots & & \vdots \\ w_{J,0} & w_{J,1} & \cdots & w_{J,I} \end{bmatrix} \begin{bmatrix} 1 \\ y_1 \\ \vdots \\ y_I \end{bmatrix}, \quad (7)
$$

where f, y_i, and $w_{j,i}$ represent an activation function, the ith input, and the weight for the jth unit multiplied by y_i, respectively. Note that these are all real-valued and that $w_{j,0}$ works as a bias added to u_j.

Equations (6) and (7) can be expressed in a vector-matrix form as

$$z = f(u) \quad (8)$$

$$u = W \begin{bmatrix} 1 \\ y \end{bmatrix}, \quad (9)$$

where each entry of y, W, u, and z are y_i, $w_{j,i}$, u_j, and z_j, respectively.

DNN has a multilayer structure. Figure 3 shows a general dense DNN where M single-layer neural networks are stacked. The output of the mth layer can be expressed as

$$z^{(m)} = f^{(m)}\left(u^{(m)}\right) \quad (10)$$

$$u^{(m)} = W^{(m)} \begin{bmatrix} 1 \\ z^{(m-1)} \end{bmatrix}, \quad (11)$$

where $[\cdot]^{(m)}$ denotes the mth layer index. $z^{(0)}$ $(= y)$ and $z^{(M)}$ $\left(= f^{(M)}\left(u^{(M)}\right)\right)$ correspond to the DNN input and output, respectively. By using nonlinear functions for f and adjusting weights appropriately, DNN can express arbitrary functions.

3.2 Application to DOA Estimation

In this paper, we use the $L \times L$ correlation matrix $\boldsymbol{R}_{xx}$ as an input to the DNN. Since $\boldsymbol{R}_{xx}$ is a Hermitian matrix, we use only the lower triangular part for the input of the DNN. Equations (10) and (11) are defined in real space. Therefore, the input vector y of the DNN is decomposed to real elements
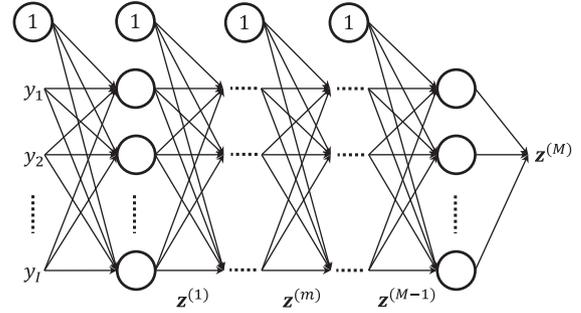
as

$$
\begin{aligned}
y = [&r_{1,1}, r_{2,2}, \ldots, r_{L,L}, \mathfrak{R}(r_{2,1}), \mathfrak{I}(r_{2,1}), \\
&\mathfrak{R}(r_{3,1}), \mathfrak{I}(r_{3,1}), \mathfrak{R}(r_{3,2}), \ldots, \mathfrak{I}(r_{L,L-1})]^T,
\end{aligned} \quad (12)
$$

where $\mathfrak{R}(\cdot)$ and $\mathfrak{I}(\cdot)$ denote the real and imaginary parts, respectively. The dimension of y, i.e., the number of inputs becomes L^2.

We define the output of DNN as the probability that an incident wave exists in each direction bin from $-60°$ to $60°$, i.e., the output is a on-grid angular spectrum. In this paper, we set the angle resolution as $1°$. Thus, DNN has 121 outputs. In the training phase, each output value is set as

$$
z_j^{(M)} = \begin{cases} 1 & \text{if a wave is incident} \\ & \text{from the } j\text{th angle bin} \\ 0 & \text{else.} \end{cases} \quad (13)
$$

Note that the estimated DOAs are determined by outputs providing K highest probabilities in all the outputs with no other restrictions for the single DNN case.

4. Evaluation of Estimation Accuracy

4.1 Simulation Conditions

We performed training and estimation simulations to evaluate the DOA estimation performance of the DNN. We use TensorFlow [18] to design and process the DNN. The following are parameters used here. The number of incident signals was two where both were narrowband signals having equal power and uncorrelated. The DOA of each signal was off-grid and ranged from $-60°$ to $60°$. The number of array elements was five, and element spacing was half-wavelength of incident signals. We used 100 snapshots of received signals to calculate the correlation matrix in each estimation.

According to the number of array elements, the number of inputs of the DNN was 25. The number of outputs of the DNN was 121 as described above. The number of intermediate layers was changed from two to five, and the number of units of each layer was selected from 121, 182, 242, 303, 363, 424, 484, 545, and 605. These correspond to $1.0, 1.5, \ldots, 5.0$ times the number of outputs. Thus, we trained 36 DNNs. The activation function of the intermediate layer was set to

a ramp function:

$$f(u) = \max(u, 0) = \begin{cases} u & \text{for } u \geq 0, \\ 0 & \text{elsewhere.} \end{cases} \quad (14)$$

The activation function of the output layer was set to standard sigmoid function:

$$f(u) = \frac{1}{1 + e^{-u}}. \quad (15)$$

Batch learning based on back propagation was applied to the DNN using 200,000 training data where each training data sample was generated by two different random DOAs within the range from −60° to 60° and white Gaussian noise. The signal-to-noise ratio (SNR) was fixed at 20 dB. Our previous study shows that the DNN trained using high SNR data provides higher performance in the same SNR range than the DNNs trained using random or low SNR data [15]. Therefore, in this paper, we fixed the SNR of the training data at 20 dB. The number of epochs and batch size were set to 999 and 128, respectively. The learning rate was changed using adaptive moment estimation (Adam) [19], which is a method to determine the rate adaptively from the past gradient, to adjust the learning rate automatically. It is known that Adam provides better DNN learning performance than other techniques such as AdaGrad [20] and AdaDelta [21]. Also, batch normalization [22], which normalizes the input to each unit to an average of 0 and a variance of 1 on a batch basis, was applied. The technique makes the training of the DNN an easier optimization problem and reduces the sensitivity to initial weights of the DNN.

During the training process, the DNN performance is validated each epoch based on the estimation success rate using 10,000 validation data which differed from training data but were generated by the same conditions as training data. The success of estimation is defined as the case where both true DOA values are included in the estimated bins (i.e., the allowable estimation error is ±0.5°). Finally, preventing the overfitting, we picked up the DNN providing the highest success rate in the validation.

In the evaluation phase, the estimation performance was evaluated using two measures: estimation success rate and RMSE:

$$\text{RMSE} = \sqrt{\frac{1}{KN} \sum_{k=1}^{K} \sum_{n=1}^{N} \left(\hat{\theta}_k^{(n)} - \theta_k^{(n)} \right)^2}, \quad (16)$$

where $[\cdot]^{(n)}$ and N denote the nth test index and the number of tests, respectively. In the following, we evaluate the performance with $N = 100,000$.

4.2 Dependency on DNN Structure

Tables 1 and 2 show estimation success rates and RMSEs for the case where we estimate two DOAs with the SNR of 20 dB using trained 36 DNNs. The definition of DNN A is

Table 1 Estimation success rate with different parameters in evaluation for DNN A.

		Number of intermediate layers			
		2	3	4	5
Number of units per intermediate layer	121	0.642	0.761	0.700	0.705
	182	0.760	0.809	0.812	0.781
	242	0.797	0.827	0.837	0.833
	303	0.810	0.831	0.834	0.834
	363	0.813	0.832	**0.837**	0.836
	424	0.813	0.836	0.836	0.828
	484	0.816	0.833	0.831	0.833
	545	0.820	0.836	0.829	0.826
	605	0.820	0.835	0.833	0.829

Table 2 RMSE [degree] with different parameters in evaluation for DNN A.

		Number of intermediate layers			
		2	3	4	5
Number of units per intermediate layer	121	9.834	3.786	5.614	5.023
	182	5.081	2.381	2.482	4.474
	242	3.886	1.807	2.007	3.824
	303	3.106	1.746	2.257	3.539
	363	3.116	1.628	1.226	2.753
	424	2.878	1.408	**1.090**	4.355
	484	2.597	1.486	1.099	2.242
	545	2.419	1.384	3.942	2.656
	605	2.325	1.477	2.482	4.581

stated below.

The DNN showing the highest success rate has four intermediate layers and each layer has 363 units. Then, the success rate is 83.7%. The lowest RMSE is 1.090° obtained when the DNN has four intermediate layers and the each layer has 424 units. They are shown in bold font in Tables 1 and 2, respectively. Although the highest success rate is achieved at a certain condition, we can obtain a reasonably accurate DNN without exact parameter optimization when the DNN has three or four intermediate layers and the number of units is not less than 242 which is twice the number of units of the output layer. We selected the DNN providing the highest success rate, i.e., the one with four intermediate layers and 363 units, for the later performance evaluation because this paper focuses on success rate performance. We label this DNN as DNN A to distinguish it from other DNNs discussed later.

Figure 4 shows the estimation success rate and RMSE of the DNN A versus the number of epochs in the training phase obtained using 10,000 validation data. Both tend to improve gradually with the progress of training. However,
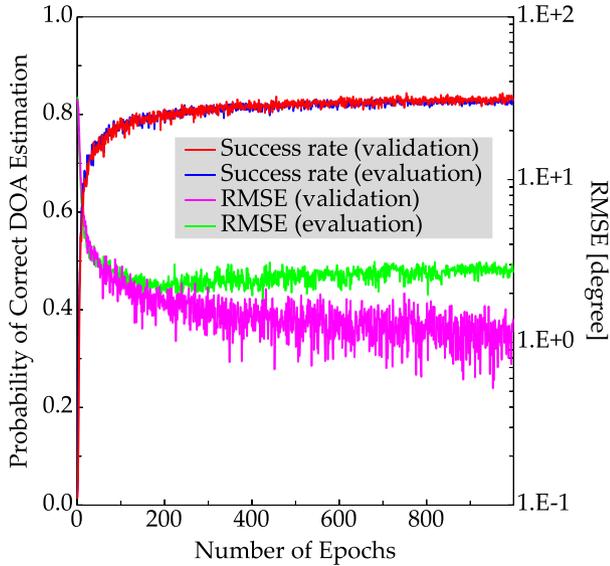
Fig. 4 Transition of estimation success rate and RMSE of DNN A in the training phase. For estimation performance confirmation, success rate and RMSE of DNN A fixed at the abscissa epoch obtained using 100,000 evaluation data are also shown.

those values fluctuate at each epoch and the last epoch does not always provide the best performance. The highest success rate is obtained where the number of epochs is 755. Therefore, the parameters of DNN A were fixed to ones at the 755th epoch. For estimation performance confirmation, the success rate and RMSE of DNN A fixed at the abscissa epoch obtained using 100,000 evaluation data are also shown in Fig. 4. The success rate curve is almost the same as one obtained by validation. On the other hand, the RMSE obtained using evaluation data becomes gradually worse from about 200 epochs. This can be regarded as overfitting in terms of the RMSE measure, and it can be said that 10,000 validation date is not enough to select the best DNN in terms of the RMSE.

4.3 Estimation Accuracy

Figures 5 and 6 show the estimation success rates and RMSEs, respectively, for the case using DNN A, i.e., the one with four intermediate layers and 363 units, Root MUSIC, and HQR†. CRB is also shown in Fig. 6. The numerical value in the parentheses in the legend indicate allowable estimation errors. The value of ±1.5° will be stated later. Note that the abscissa represents SNR for the estimation phase, not for the learning one. For Root MUSIC, we assume that the number of incident signals is known.

As shown in Table 1, the success rate of DNN A is 83.7% at the SNR of 20 dB. As described above, the success of estimation means that the estimation error is within ±0.5°. When the same requirement is applied, i.e., the allowable estimation error is set to ±0.5° for the Root MUSIC, the

---

†Hyperparameters of HQR, μ, ϵ, and p in [6] were empirically set to 10, 3×10^{-6}, and 3×10^{-6}, respectively.
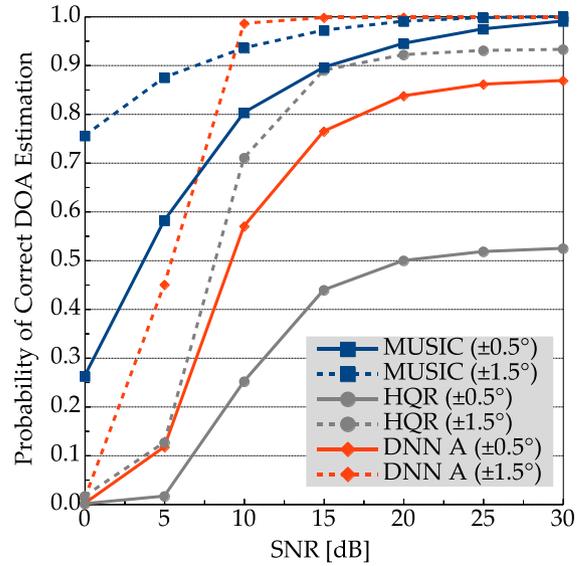
Fig. 5 Success rates of the DNN A, Root MUSIC, and HQR. As a special case, success rates when ±1.5° is allowed are also shown.
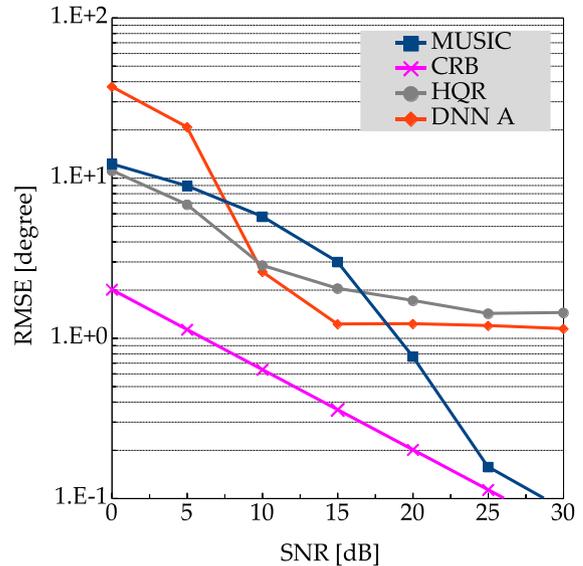
Fig. 6 RMSEs of DNN A, Root MUSIC, HQR, and CRB.

success rate for the Root MUSIC becomes higher than 90% at the SNR of 20 dB. The RMSE of DNN A is smaller than the that of Root MUSIC at the SNR of 10 dB and 15 dB. However, it converges at about 1.2° and the RMSE of Root MUSIC becomes smaller again than the that of DNN A at the SNR of 20 dB or higher. To discuss this performance difference, let us examine an example when DNN A failed the DOA estimation, i.e., the estimation error was larger than the allowable range.

Figure 7 shows an example of the output of DNN A. The estimated DOAs were −2° and 10° although true DOAs are −2.21° and 9.49°. In this case, the estimation error of the latter DOA is beyond the allowable estimation error ±0.5°. This is caused because the DOA of 9.49° is almost on the
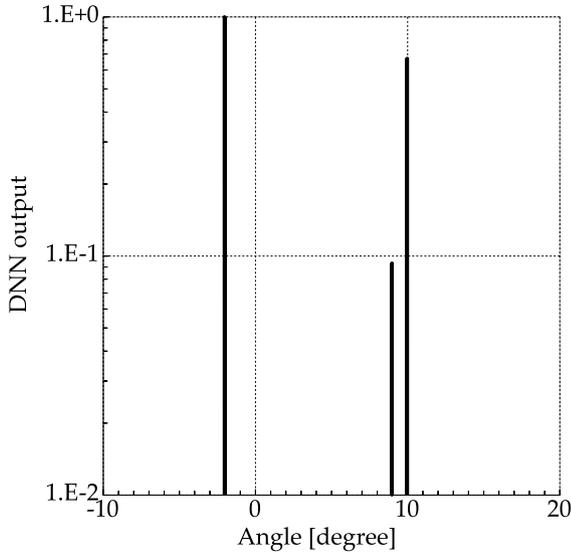
Fig. 7 Output example of DNN A when estimation fails. True DOAs: −2.21° and 9.49°, estimated DOAs: −2° and 10°.

Fig. 8 Staggered grids of DNN A and DNN B.

boundary of bins of 9° and 10°. Thus, it is supposed that estimation errors of more than ±0.5° may be often observed when one or both of DOAs are on the boundary of bins.

To confirm our surmise, the success rates when the allowable estimation error is ±1.5° are also shown in Fig. 5 as a special case. The success rate of DNN A for this relaxed condition is highly increased and reaches about 100% at the SNR of 15 dB. Note that this success rate is better than that of Root MUSIC. So, we can conclude that the DOA estimation using DNN A has a possibility achieving very accurate estimation performance if we solve the on-grid related issue.

The success rates of HQR are lower than those of Root MUSIC and DNN A even when the allowable estimation error is ±1.5°. Multi-band expansion may be needed to obtain higher performance as in [6].

4.4 Proposed Solution for the On-Grid Related Issue

As described above, it is shown that the DNN frequently fails to estimate the correct bin when a signal arrives at angles near the grid border. One approach of solving this on-grid related issue is to reconstruct the DNN as a regression model rather than a classification model [14]. In this case, each output unit of the DNN gives the estimated DOA angle directly. Thus, the regression-based DNN can estimate off-grid DOAs and this grid-border problem does not occur.

However, the regression-based approach has different problems. The structure of the output layer must be changed depending on the number of incident signals. In addition, the training complexity of the DNN increases with the number of incident signals since the DOA output order may change the training performance in spite of the fact that the DOA output order has no meaning for the accuracy.

Another approach is to make the angle resolution smaller than 1°. However, in this case, the number of units of each layer may increase in inverse proportion to the reso-

lution, and the training time and difficulty may also increase. Moreover, the on-grid related issue shown in Sect. 4.3 is still unavoidable even if the resolution is reduced.
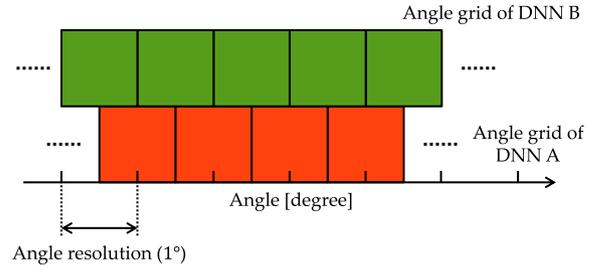
Here, we propose a method using another DNN (labeled DNN B) which has a grid shifted half the grid spacing from the that of DNN A and combining these two DNNs in order to reduce the estimation error caused by the on-grid related issue. The grids of DNN A and DNN B are staggered as shown in Fig. 8. In the estimation phase, the DOAs are determined by searching peaks in the combined angular spectrum of DNN A and DNN B. The DNN B can be trained independently at almost the same cost as DNN A. Note that the DNN B has 122 output units from −60.5° to 60.5° to cover the output range of DNN A.

4.5 Verification of the Proposed Method

We trained and validated 36 DNNs to determine configuration and parameters of DNN B. The DOA of each signal is ranged from −60.5° to 60.5°. The number of units of each layer was selected from 122, 183, 244, 305, 366, 427, 488, 549, and 610. These correspond to 1.0, 1.5, . . . , 5.0 times the number of outputs. The other conditions were the same as those in Sect. 4.1. Tables 3 and 4 show estimation success rates and RMSEs for the case where we estimate two DOAs with the SNR of 20 dB using trained 36 DNNs.

The DNN showing the highest success rate has three intermediate layers and each layer has 366 units. Then, the success rate is 83.8%. The lowest RMSE is 0.976° obtained when the DNN has five intermediate layers and each layer has 488 units. They are shown in bold font in Tables 3 and 4, respectively. We use the DNN showing the highest success rate, i.e., the one with three intermediate layers and 366 units, as the DNN B.

Figures 9 and 10 show the estimation success rates and RMSEs of DNN A, DNN B, staggered combination of these DNNs, and Root MUSIC as a baseline. Note that "MUSIC" and "DNN A" in Figs. 9 and 10 are the same as "MUSIC (±0.5°)" and "DNN A (±0.5°)" in Figs. 5 and 6, respectively. CRB is also shown in Fig. 10.

In addition to the above DNNs, we tested another DNN (DNN H) whose angle resolution is 0.5° (half grid size). The estimation success rate and RMSE of DNN H are also shown in Figs. 9 and 10. This DNN has 241 output units from −60° to 60°, five intermediate layers, and each layer has 603 units which is 2.5 times the number of the outputs.

Table 3 Estimation success rate with different parameters in evaluation for DNN B.

		Number of intermediate layers			
		2	3	4	5
Number of units per intermediate layer	122	0.644	0.631	0.699	0.761
	183	0.689	0.769	0.758	0.761
	244	0.786	0.823	0.835	0.835
	305	0.809	0.830	0.836	0.834
	366	0.812	**0.838**	0.834	0.836
	427	0.821	0.831	0.830	0.836
	488	0.821	0.836	0.833	0.827
	549	0.822	0.833	0.829	0.830
	610	0.822	0.833	0.826	0.830

Table 4 RMSE [degree] with different parameters in evaluation for DNN B.

		Number of intermediate layers			
		2	3	4	5
Number of units per intermediate layer	122	11.14	7.846	7.041	5.073
	183	8.952	3.886	4.941	8.005
	244	4.545	2.131	1.544	5.474
	305	3.116	1.708	1.416	5.246
	366	2.760	1.595	4.119	3.269
	427	2.551	1.487	3.129	3.563
	488	2.719	1.399	1.885	**0.976**
	549	2.440	1.450	1.079	3.078
	610	2.487	1.402	1.347	2.849

Fig. 9 Success rates of DNN A, DNN B, staggered combination of DNN A and DNN B, DNN H, and Root MUSIC.
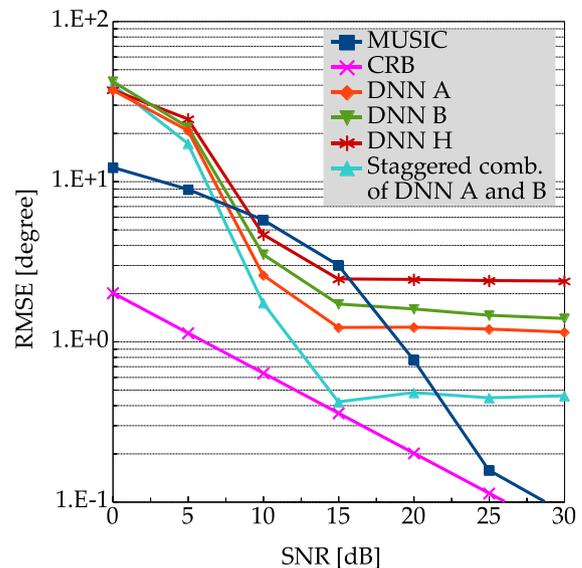
Fig. 10 RMSEs of DNN A, DNN B, staggered combination of DNN A and DNN B, DNN H, Root MUSIC, and CRB.

These parameters were determined in a similar manner as DNN A.

Although the success rates of DNN A and DNN B are almost equal and overlapped as shown in Fig. 9, the RMSEs of DNN A and DNN B are different as in Fig. 10. This is because the success rate and RMSE at each epoch in the training phase fluctuate individually as shown in Fig. 4 and the epoch providing the highest success rate does not always provide the small RMSE.

Compared with Root MUSIC, DNN A and DNN B have lower success rates than the that of Root MUSIC over all the SNR range. However, the success rate of the proposed method, i.e., staggered combination of DNN A and DNN B is higher than the that of Root MUSIC at the SNR of 15 dB or higher and reaches 99% at the SNR of 20 dB or higher. DNN H shows much higher success rates than those of DNN A and DNN B at the SNR of 10 dB or higher. However, the success rate of the proposed method is slightly higher than that of DNN H. The RMSE is significantly improved compared with the single use cases of DNN A, DNN B, and DNN H. It implies that most of estimation

errors caused by the bin boundary problem are effectively resolved by our proposed method. Note that the RMSE of the proposed method is about 0.4° at the SNR of 15 dB and is close to CRB.

Figure 11 shows an example of the combined angular spectrum of DNN A and DNN B. In this example, the signals arrive from −2.21° and 9.49° as in Fig. 7. The second peak of DNN A is 10°, and thus DNN A fails to estimate 9°, which is the correct unit including 9.49°. On the other hand, the proposed method succeeds in estimating this signal because DNN B outputs higher probability at 9.5° than that of DNN A at 10°.

It was also confirmed that the estimation failed when
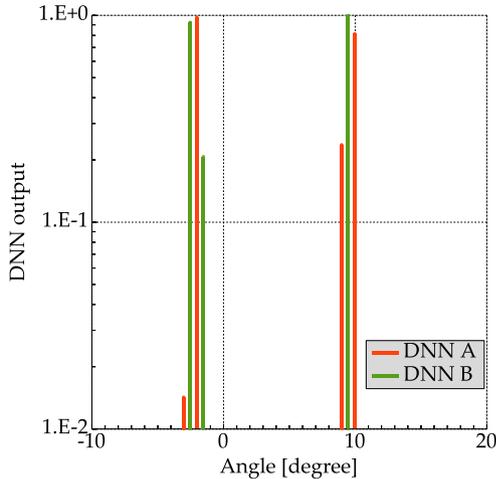
Fig. 11 An example of combined angular spectrum of DNN A and DNN B. True DOAs are $-2.21°$ and $9.49°$. Output units: $-2°$ and $9.5°$ are selected correctly by searching peaks in this spectrum.

Table 5 Estimation success rate with different parameters in evaluation for the case of $1°$ DOA difference for DNN C.

		Number of intermediate layers			
		2	3	4	5
Number of units per intermediate layer	121	0.959	0.961	0.959	0.959
	182	0.962	0.963	0.961	0.961
	242	0.961	0.962	0.961	0.962
	303	0.961	0.961	0.960	0.959
	363	0.962	0.962	0.963	0.962
	424	0.960	0.962	**0.963**	0.960
	484	0.961	0.962	0.962	0.960
	545	0.961	0.962	0.962	0.962
	605	0.960	0.962	0.961	0.961

Table 6 Estimation success rate with different parameters in evaluation for the case of $1°$ DOA difference for DNN D.

		Number of intermediate layers			
		2	3	4	5
Number of units per intermediate layer	122	0.957	0.958	0.961	0.957
	183	0.960	0.962	0.962	0.961
	244	0.958	0.961	0.961	0.962
	305	0.959	**0.963**	0.961	0.959
	366	0.962	0.959	0.959	0.961
	427	0.962	0.963	0.961	0.962
	488	0.962	0.961	0.962	0.959
	549	0.960	0.961	0.961	0.960
	610	0.962	0.962	0.962	0.959

two signals arrived from similar directions. The RMSE of the proposed method fluctuates slightly at the SNR of 15 dB or higher in Fig. 10 because there were a few special cases where an output bin far away from the true DOA was estimated due to failing in separating such proximity signals. In success rate evaluation, any error of $0.5°$ or higher is regarded as a failure, whereas a large error in the angle domain has a big impact on RMSE.

4.6 Close DOA Scenario

The feature that DNN can be trained for specific scenarios is unique to machine-learning-based methods. In order to reduce the estimation error occurring when two signals arrive from close directions, we design a DNN suitable to estimate the special case $|\theta_1 - \theta_2| = 1°$ similar to our previous evaluation under an on-grid DOA scenario [15]. We trained 36 DNNs each for DNN A and DNN B with an additional restriction of $|\theta_1 - \theta_2| = 1°$. Hereinafter, we call these DNNs DNN C and DNN D, respectively.

Tables 5 and 6 show estimation success rates for DNN C and DNN D tested and validated using data with $|\theta_1 - \theta_2| = 1°$ at the SNR of 20 dB. In the following, we used the DNNs providing the highest success rate where the number of intermediate layers was four and the each layer had 424 units as shown in Table 5 for DNN C and where the number of intermediate layers was three and the each layer had 305 units as shown in Table 6 for DNN D.

Figures 12 and 13 show the estimation success rates and RMSEs for the case of $1°$ DOA difference. The success rates of DNN C and DNN D are 97.3% and 97.6%, respectively, at the SNR of 30 dB whereas the that of Root MUSIC is 47.9% which is less than half of the success rates of DNN C and DNN D. The success rates at the SNR of 0 dB and 5 dB differ between DNN C and DNN D because DNN C has more layers and units than DNN D. Our several evaluation results show that the estimation accuracy at the low SNR is highly

affected by the number of layers and the number of units. Thus, it might be important to select an appropriate SNR condition for training. Note that the RMSEs of DNN C and DNN D converge to $0.291°$ which is close to the lower bound, $1/\sqrt{12} \approx 0.289°$, when the DOA distribution is uniform.

However, this RMSE performance should be considered too optimistic since we tested the DNN C and DNN D based on the prior knowledge of $1°$ DOA difference. Actually, the RMSEs of these DNNs at the SNR of 10 dB or higher are much lower than CRB. In general, we cannot know the DOA difference in advance. As described next subsection, these DNNs do not work well when there is no restriction in DOA difference. However, the feature that the estimation accuracy can be improved if the DOA difference is known or able to be estimated is advantageous to machine-learning-based methods.

On the other hand, the success rate of the staggered combination of DNN C and DNN D becomes smaller than the that of Root MUSIC at the SNR of 30 dB. In fact, it is
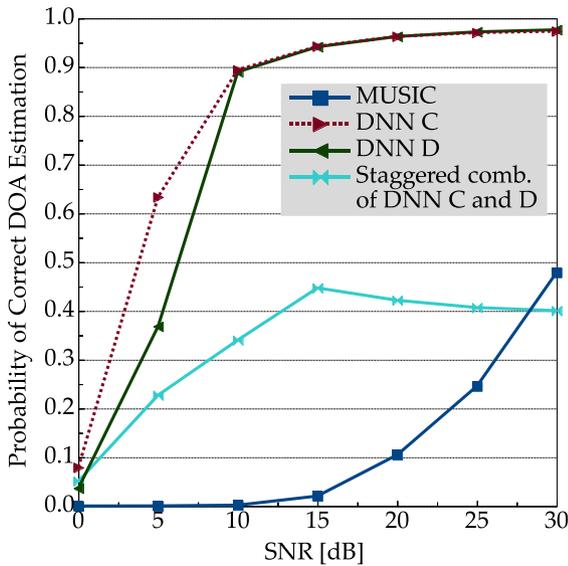
Fig. 12 Success rates of several types of DNNs and Root MUSIC for the case of 1° DOA difference.
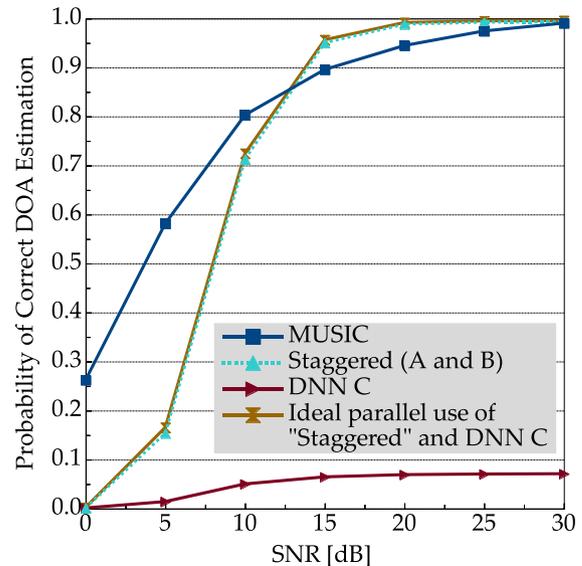
Fig. 14 Success rates for the case switching the staggered combination of DNN A and DNN B or DNN C ideally.
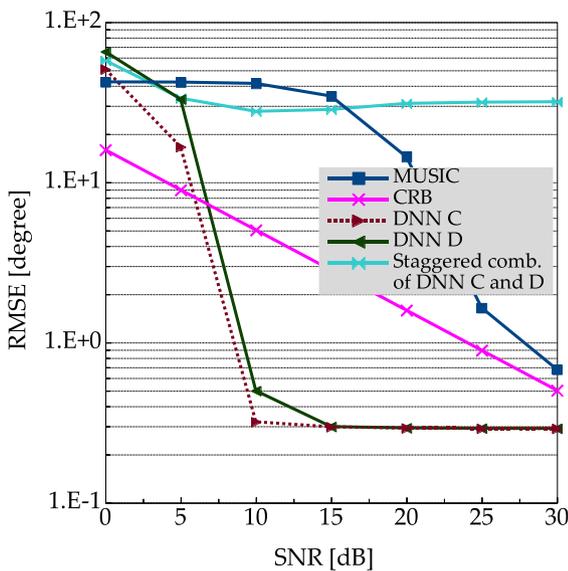
Fig. 13 RMSEs of several types of DNNs, Root MUSIC, and CRB for the case of 1° DOA difference.
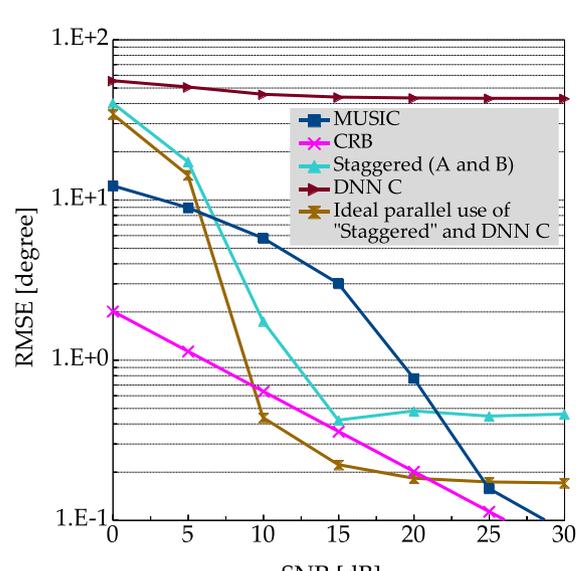
Fig. 15 RMSEs for the case switching the staggered combination of DNN A and DNN B or DNN C ideally.

frequently observed that the combined angular spectrum with the resolution of 0.5° shows only one peak near the DOAs. Therefore, it can be said that the staggered combination is not a good choice when the DOA difference is so small.

4.7 Ideal Use of DNN A, DNN B, and DNN C

As described above, the staggered combination of DNN C and DNN D is not suitable for the severe condition of 1° DOA difference. Instead, two single DNN, i.e., DNN C and DNN D achieve the success rate higher than 97%. Therefore, we verify a possibility of ideal use of DNN A, DNN B, and DNN C in the the case where no DOA restriction is assumed as in Sect. 4.5. Here, DNN A and DNN B are combined in

the angular spectrum domain as the best choice for the case where the DOA difference is not so small. On the other hand, for the case of proximity signals, it is better to use DNN C (or DNN D) alone. In the following, we simply take either set of the estimated DOAs of the staggered combination of DNN A and DNN B or DNN C which provides lower sum of squared errors calculated using the correct DOAs.

Figures 14 and 15 show the success rates and RMSEs for the single and parallel use cases of the staggered ones and DNN C. "MUSIC" in Figs. 14 and 15 are the same as "MUSIC (±0.5°)" in Figs. 5 and 6, respectively. Similarly, "Staggered (A and B)" in Figs. 14 and 15 are the same as "Staggered comb. of DNN A and B" in Figs. 9 and 10, re-

spectively.

Since DNN C is trained only for the case of $|\theta_1 - \theta_2| = 1°$, the success rate of DNN C is much lower than that of others. The best selection case of the staggered ones or DNN C shows a slightly-better success rate than only the staggered ones. However, as mentioned in Sect. 4.5, the RMSE of the ideal use case is visibly improved in any SNR compared with the single use cases of the staggered ones and DNN C. This result clearly shows the possibility of performance improvement by parallel use of specially-trained DNNs. The RMSEs of the ideal use case at the SNR of 10 dB and 15 dB are lower than CRB because the best estimated DOA set is ideally selected based on the correct DOAs. The results based on a trial selecting the DOA set are shown in Appendix.

5. Conclusion

In this paper, we evaluated a DOA estimation method using deep learning in the case where two narrowband signals of equal power are incident on a uniform linear array from off-grid angles. Computer simulations have indicated high estimation accuracy of the DNN equal to or higher than Root MUSIC when we allow single-bin error. To reduce the estimation error, we proposed a method of combining two DNNs that the grids of them are off by half the resolution. The success rate of this staggered DNN combination is higher than that of Root MUSIC at the SNR of 15 dB or higher and reaches 99% at the SNR of 20 dB or higher. It is also confirmed that most of estimation errors at high SNR regions are caused by the bin boundary problem and that the staggered combination is an effective solution to this problem.

In addition, we designed a DNN suitable to the case where two signals are incident with close DOAs and examined the parallel use of staggered combination and the specially-designed DNN. It has been indicated that the DNN designed for the specific scenario achieves the success rate of 97.6% and that the integrated use of specialized DNN improves the DOA estimation performance.

Currently, the computational load of the matrix-vector multiplications required by DNN ($O(IJ)$; $IJ = 363^2 = 131,769$ in DNN A) is heavier than the that of the eigenvalue decomposition required by MUSIC ($O(L^3)$; $L^3 = 5^3 = 125$). If such a computational complexity is allowed, DNN-based DOA estimation will be definitely a useful and accurate choice. Further optimization of the DNN model is an urgent issue.

Acknowledgments

References

[1] Y. Kase, T. Nishimura, T. Ohgane, Y. Ogawa, D. Kitayama, and Y. Kishiyama, "Performance analysis of DOA estimation of two targets using deep learning," Proc. WPMC 2019, Nov. 2019, DOI: 10.1109/WPMC48795.2019.9096165.

[2] Y. Kase, T. Nishimura, T. Ohgane, Y. Ogawa, T. Sato, D. Kitayama, and Y. Kishiyama, "A consideration on accuracy improvement in DOA estimation of two targets with deep learning," Proc. ICETC 2020, P1-3, Dec. 2020, DOI: 10.34385/proc.63.P1-3.

[3] H. Krim and M. Viberg, "Two decades of array signal processing research: the parametric approach," IEEE Sig. Process. Mag., vol.13, no.4, pp.67–94, July 1996, DOI: 10.1109/79.526899.

[4] A. Massa, P. Rocca, and G. Oliveri, "Compressive sensing in electromagnetics — A review," IEEE Antennas Propag. Mag., vol.57, no.1, pp.224–238, Feb. 2015, DOI: 10.1109/MAP.2015.2397092.

[5] K. Hayashi, M. Nagahara, and T. Tanaka, "A user's guide to compressed sensing for communications systems," IEICE Trans. Commun., vol.E96-B, no.3, pp.685–712, March 2013, DOI: 10.1587/transcom.E96.B.685.

[6] T. Terada, T. Nishimura, Y. Ogawa, T. Ohgane, and H. Yamada, "DOA estimation for multi-band signal sources using compressed sensing techniques with Khatri-Rao processing," IEICE Trans. Commun., vol.E97-B, no.10, pp.2110–2117, Oct. 2014, DOI: 10.1587/transcom.E97.B.2110.

[7] G.E. Hinton, S. Osindero, and Y. Teh, "A fast learning algorithm for deep belief nets," Neural Comput., vol.18, no.7, pp.1527–1544, July 2006, DOI: 10.1162/neco.2006.18.7.1527.

[8] G.E. Hinton and R. Salakhutdinov, "Reducing the dimensionality of data with neural networks," Science, vol.313, no.5786, pp.504–507, July 2006, DOI: 10.1126/science.1127647.

[9] R. Takeda and K. Komatani, "Sound source localization based on deep neural networks with directional activate function exploiting phase information," Proc. IEEE ICASSP 2016, pp.405–409, March 2016, DOI: 10.1109/icassp.2016.7471706.

[10] W. Liu, J. Xin, W. Zuo, J. Li, N. Zheng, and A. Sano, "Deep learning based localization of near-field sources with exact spherical wavefront model," Proc. Eur. Signal Process. Conf. (EUSIPCO), pp.1–5, Sept. 2019, DOI: 10.23919/EUSIPCO.2019.8903003.

[11] H. Huang, J. Yang, H. Huang, Y. Song, and G. Gui, "Deep learning for super-resolution channel estimation and DOA estimation based massive MIMO system," IEEE Trans. Veh. Technol., vol.67, no.9, pp.8549–8560, Sept. 2018, DOI: 10.1109/TVT.2018.2851783.

[12] Z. Liu, C. Zhang, and P.S. Yu, "Direction-of-arrival estimation based on deep neural networks with robustness to array imperfections," IEEE Trans. Antennas Propag., vol.66, no.12, pp.7315–7327, Dec. 2018, DOI: 10.1109/TAP.2018.2874430.

[13] D. Hu, Y. Zhang, L. He, and J. Wu, "Low-complexity deep-learning-based DOA estimation for hybrid massive MIMO systems with uniform circular arrays," IEEE Wirel. Commun. Lett., vol.9, no.1, pp.83–86, Jan. 2020, DOI: 10.1109/LWC.2019.2942595.

[14] Y. Cao, T. Lv, Z. Lin, P. Huang, and F. Lin, "Complex ResNet aided DoA estimation for near-field MIMO systems," IEEE Trans. Veh. Technol., vol.69, no.10, pp.11139–11151, Oct. 2020, DOI: 10.1109/TVT.2020.3007894.

[15] Y. Kase, T. Nishimura, T. Ohgane, Y. Ogawa, D. Kitayama, and Y. Kishiyama, "Fundamental trial on DOA estimation with deep learning," IEICE Trans. Commun., vol.E103-B, no.10, pp.1127–1135, Oct. 2020, DOI: 10.1587/transcom.2019EBP3260.

[16] B.D. Rao and K.V.S. Hari, "Performance analysis of Root-MUSIC," IEEE Trans. Acoust., Speech, Signal Process., vol.37, no.12, pp.1939–1949, Dec. 1989, DOI: 10.1109/29.45540.

[17] P. Stoica and A. Nehorai, "MUSIC, maximum likelihood, and Cramer-Rao bound," IEEE Trans. Acoust., Speech, Signal Process., vol.37, no.5, pp.720–741, May 1989, DOI: 10.1109/29.17564.

[18] M. Abadi, A. Agarwal, P. Barham, E. Brevdo, Z. Chen, C. Citro, G.S. Corrado, A. Davis, J. Dean, M. Devin, S. Ghemawat, I. Goodfellow, A. Harp, G. Irving, M. Isard, Y. Jia, R. Jozefowicz, L. Kaiser, M. Kudlur, J. Levenberg, D. Mane, R. Monga, S. Moore, D. Murray, C. Olah, M. Schuster, J. Shlens, B. Steiner, I. Sutskever, K. Talwar,

P. Tucker, V. Vanhoucke, V. Vasudevan, F. Viegas, O. Vinyals, P. Warden, M. Wattenberg, M. Wicke, Y. Yu, and X. Zheng "TensorFlow: Large-scale machine learning on heterogeneous distributed systems," arXiv:1603.04467v2, March 2016.

[19] D.P. Kingma and J.L. Ba, "Adam: A method for stochastic optimization," arXiv:1412.6980v9, Jan. 2017.

[20] J. Duchi, E. Hazan, and Y. Singer, "Adaptive subgradient methods for online learning and stochastic optimization," Journal of Machine Learning Research, vol.12, pp.2121–2159, July 2011.

[21] M.D. Zeiler, "ADADELTA: An adaptive learning rate method," arXiv:1212.5701v1, Dec. 2012.

[22] S. Ioffe and C. Szegedy, "Batch normalization: Accelerating deep network training by reducing internal covariate shift," arXiv:1502.03167v3, March 2015.

Appendix: A DNN Selection Trial

Here, we show the results of selecting a set of estimated DOAs from the staggered combination of DNN A and DNN B or DNN C using another DNN to detect 1° DOA difference. We used the input vector (12) for this close-DOA-detection DNN, which is the same as the input vector for DNN A, DNN B, and DNN C. The intermediate layers were also the same as those described in Sect. 4.1. We allocated two output units corresponding to the 1° DOA difference case and the other case. The output of the DNN was set to the probability of the case. Since the desired output was one-hot, the activation function of the output layer was set to a softmax function:

$$z_j^{(M)} = \frac{\exp\left(u_j^{(M)}\right)}{\sum_{j=1}^{J} \exp\left(u_j^{(M)}\right)}. \tag{A·1}$$

In the training phase, 100,000 random DOA difference data and 100,000 1° DOA difference data were used. The SNR was randomly set within the range from 0 dB to 30 dB. As a result of the training, the DNN showing the highest detection success rate (99.2%) had five intermediate layers and each layer had 545 units.

Figures A·1 and A·2 show the DOA estimation success rates and RMSEs for the case switching the staggered combination of DNN A and DNN B or DNN C based on close DOA detection. The success rate of switching the staggered ones or DNN C based on the close DOA detection are slightly degraded in any SNR compared with the single use cases of the staggered ones. However, the RMSE is visibly improved compared with the staggered ones and is close to that of the ideal selection case of the staggered ones or DNN C at the SNR of 25 dB and 30 dB. It is highly expected that the degradation of the success rate can be reduced by improving the detection success rate in the future study.
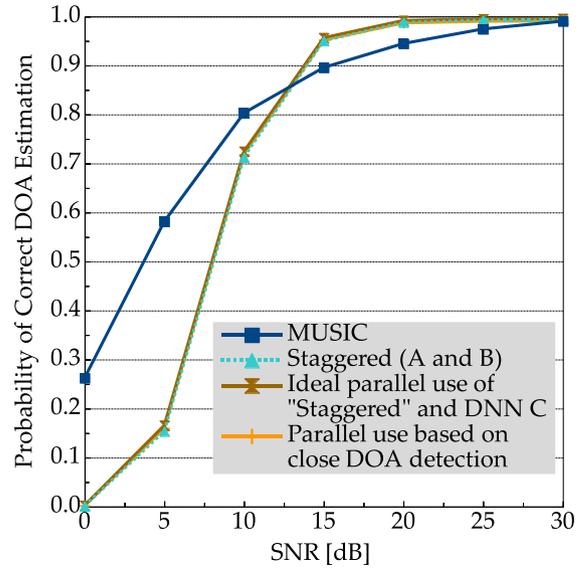
Fig. A·1 Success rates for the case switching the staggered combination of DNN A and DNN B or DNN C based on close DOA detection.
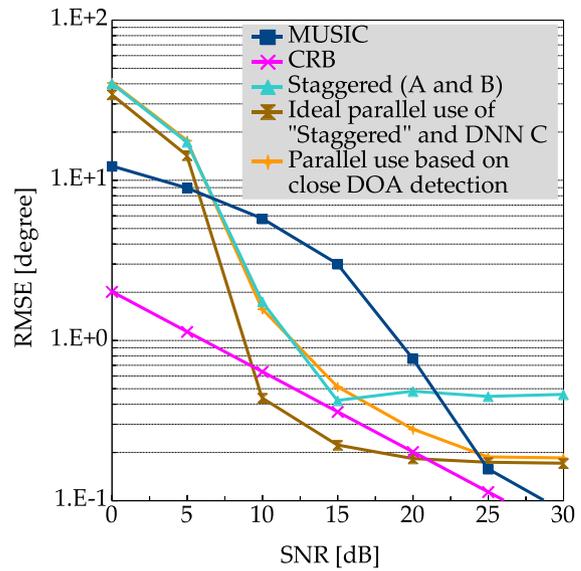
Fig. A·2 RMSEs for the case switching the staggered combination of DNN A and DNN B or DNN C based on close DOA detection.

Yuya Kase received a B.E. degree in electrical and electronic engineering from National Institute of Technology, Asahikawa College, Asahikawa, Japan, in 2017 and the M.E. degree in the field of media and network technologies from Hokkaido University, Sapporo, Japan, in 2019. He is currently a Ph.D. student at Hokkaido University. His interests are DOA estimation and mobile communication.

Toshihiko Nishimura received the B.S. and M.S. degrees in physics and Ph.D. degree in electronics engineering from Hokkaido University, Sapporo, Japan, in 1992, 1994, and 1997, respectively. Since 1998, he has been with Hokkaido University, where he is currently an Associate Professor. His current research interests are in MIMO systems using smart antenna techniques. He received the Young Researchers' Award of IEICE in 2000, the Best Paper Award from IEICE in 2007, and TELECOM System Technology Award from the Telecommunications Advancement Foundation of Japan in 2008, the best magazine paper award from IEICE Communications Society in 2011, and the Best Tutorial Paper (in Japanese) Award from the IEICE Communications Society in 2018. He is a member of the IEEE.

Takeo Ohgane received the B.E., M.E., and Ph.D. degrees in electronics engineering from Hokkaido University, Sapporo, Japan, in 1984, 1986, and 1994, respectively. From 1986 to 1992, he was with Communications Research Laboratory, Ministry of Posts and Telecommunications. From 1992 to 1995, he was on assignment at ATR Optical and Radio Communications Research Laboratory. Since 1995, he has been with Hokkaido University, where he is currently a Professor. During 2005–2006, he was at Centre for Communications Research, University of Bristol, U.K., as a Visiting Fellow. His research interests are in MIMO signal processing for wireless communications. He received the IEEE AP-S Tokyo Chapter Young Engineer Award in 1993, the Young Researchers' Award of IEICE in 1990, the Best Paper Award from IEICE in 2007, TELECOM System Technology Award from the Telecommunications Advancement Foundation of Japan in 2008, the Best Magazine Paper Award from IEICE Communications Society in 2011, and the Best Tutorial Paper (in Japanese) Award from IEICE Communications Society in 2018. He is a member of the IEEE.

Yasutaka Ogawa received the B.E., M.E., and Ph.D. degrees from Hokkaido University, Sapporo, Japan, in 1973, 1975, and 1978, respectively. Since 1979, he has been with Hokkaido University, where he is currently a Professor Emeritus. During 1992–1993, he was with ElectroScience Laboratory, the Ohio State University, as a Visiting Scholar, on leave from Hokkaido University. His professional expertise encompasses super-resolution estimation techniques, applications of adaptive antennas for mobile communication, multiple-input multiple-output (MIMO) techniques, and measurement techniques. He proposed a basic and important technique for time-domain super-resolution estimation for electromagnetic wave measurement such as antenna gain measurement, scattering/diffraction measurement, and radar imaging. Also, his expertise and commitment to advancing the development of adaptive antennas contributed to the realization of space division multiple accesses (SDMA) in the Personal Handy-phone System (PHS). He received the Yasujiro Niwa Outstanding Paper Award in 1978, the Young Researchers' Award of IEICE in 1982, the Best Paper Award from IEICE in 2007, TELECOM system technology award from the Telecommunications Advancement Foundation of Japan in 2008, the Best Magazine Paper Award from IEICE Communications Society in 2011, the Achievement Award from IEICE in 2014, and the Best Tutorial Paper (in Japanese) Award from IEICE Communications Society in 2018. He also received the Hokkaido University Commendation for excellent teaching in 2012. He is a Fellow of the IEEE.

Takanori Sato received the Ph.D. degree in the field of media and network technologies from Hokkaido University, Japan, in 2018. He was a Research Fellow of Japan Society for the Promotion of Science (JSPS) from 2017 to 2019. In 2019, he moved to University of Hyogo as an assistant professor. He is currently an associate professor in Hokkaido University. His research interests include the theoretical and numerical studies of optical fibers and photonic circuits using the coupled mode theory and the finite element method. He is a member of the Japan Society of Applied Physics (JSAP), Institute of Electrical and Electronics Engineers (IEEE), and the Optical Society of America (OSA).

Yoshihisa Kishiyama received his B.E., M.E., and Ph.D. degrees from Hokkaido University, Sapporo, Japan in 1998, 2000, and 2010, respectively. He is now a Senior Research Engineer of 5G Laboratory in NTT DOCOMO, INC. Since he joined NTT DOCOMO in 2000, he has been involved in research and development on 4G/5G radio access technologies and physical layer standardization in 3GPP. In 2012, he received the International Telecommunication Union Association of Japan (ITU-AJ) Award for contributions to LTE.